

Charge density waves in infinite-layer NdNiO₂ nickelates

Charles C. Tam,^{1,2,*} Jaewon Choi,^{1,*} Xiang Ding,^{3,*} Stefano Agrestini,¹ Abhishek Nag,^{1,4} Bing Huang,⁵ Huiqian Luo,^{6,7} Mirian García-Fernández,¹ Liang Qiao,^{3,†} and Ke-Jin Zhou^{1,‡}

¹*Diamond Light Source, Harwell Campus, Didcot OX11 0DE, United Kingdom.*

²*H. H. Wills Physics Laboratory, University of Bristol, Bristol BS8 1TL, United Kingdom.*

³*School of Physics, University of Electronic Science and Technology of China, Chengdu, 610054, China*

⁴*Laboratory for Non-linear Optics, Paul Scherrer Institut, CH-5232 Villigen, PSI, Switzerland*

⁵*Beijing Computational Science Research Center, Beijing 100193, China*

⁶*Beijing National Laboratory for Condensed Matter Physics,
Institute of Physics, Chinese Academy of Sciences, Beijing 100190*

⁷*Songshan Lake Materials Laboratory, Dongguan, Guangdong 523808, China*

(Dated: December 9, 2021)

In materials science, replicating superconductivity in chemical compositions with a cuprate-like structure is a long-sought research quest. Recently it was successfully realised in the superconducting infinite-layer nickelates. Although differing from cuprates in electronic and magnetic properties, strong Coulomb interactions suggest infinite-layer nickelates have a propensity to various symmetry-breaking orders that populate in cuprates. Here we report the observation of charge density waves (CDWs) in infinite-layer NdNiO₂ films using Ni-*L*₃ resonant x-ray scattering. Remarkably, CDWs form in Nd 5*d* and Ni 3*d* orbitals at the same commensurate wavevector (0.333, 0) *r.l.u.*, with non-negligible out-of-plane dependence, and a correlation length up to 80 Å. Spectroscopic studies reveal a strong connection between CDWs and the Nd 5*d* - Ni 3*d* orbital hybridization. Upon entering the superconducting state at 20% Sr doping, the CDWs disappear. Our work demonstrates the existence of CDWs in infinite-layer nickelates with a multi-orbital character distinct to cuprates, establishing a unique low-energy physics.

The realisation of superconducting infinite-layer nickelates marks the latest milestone in the field of high-temperature superconductivity research [1–6]. Being isostructural to CaCuO₂, infinite-layer nickelates contain quasi-two-dimensional (2D) NiO₂ layers, nominal 3*d*⁹ Ni¹⁺ ions with spin *S* = 1/2, and an active *d*_{*x*²−*y*²} orbital near the Fermi level, analogous to the cuprate family of high temperature superconductors [7, 8]. However, X-ray absorption (XAS) and electron energy loss spectroscopies have shown their electronic structures are closer to the Mott-Hubbard than the charge-transfer regime, distinct from cuprates [9–11]. Another distinctive feature when comparing to cuprates is the three-dimensional (3D) itinerant 5*d* bands of the rare-earth ions are predicted to hybridize with the localized 2D Ni-O bands [8, 10, 12]. This strong hybridization is corroborated by resonant inelastic X-ray scattering (RIXS) where Nd 5*d* - Ni 3*d* hybridized states were observed [10], as well as a change in sign of low temperature Hall coefficient as a function of Sr doping, indicating the presence of two bands at the Fermi level [2, 3]. On the other hand, although the magnetism of infinite-layer nickelates is under debate [13–15], Nd_{1−*x*}Sr_{*x*}NiO₂, grown on and capped with SrTiO₃ (STO), shows well defined and highly dispersive magnetic excitations, validating the existence of strong electron Coulomb interaction in infinite-layer nickelates, in particular, the proximity between the strong antiferromagnetic (AFM) correlations and superconductivity [16]. The strong electronic and AFM correlations are key ingredients that give rise to symmetry breaking orders, such as the spin density waves (SDWs), or charge den-

sity waves (CDWs), which are relevant to superconductivity in cuprates [17, 18]. A natural question is whether these ordered states are present in infinite-layer nickelates. In this study, we applied Ni *L*₃-edge XAS and RIXS to NdNiO₂ thin films and revealed the presence of CDWs. We show that there is a clear correlation between the CDWs and the hybridized Nd 5*d* - Ni 3*d* orbital, demonstrating the active participation of the rare-earth 5*d* states in nickelates low-energy physics.

Nd_{1−*x*}Sr_{*x*}NiO₂ thin films were prepared by pulsed laser deposition and subsequently topotactic reduction, similar to that applied in Refs. [1, 3] but without STO capping layers (see Methods). One of the reduced parent NdNiO₂ films, referred as 'NNO₂-1' hereafter, features a two-peak Ni *L*₃ XAS profile consistent to those in LaNiO₂ and NdNiO₂ reported recently [10, 19]. The first peak (denoted A') reflects the transition to the Nd 5*d*-Ni 3*d* hybridized states and the second peak (denoted A) detects the main absorption from 2*p*_{3/2}⁶3*d*⁹ to 2*p*_{3/2}⁵3*d*¹⁰ transition at the nominal Ni¹⁺ sites (Figs. 1a, b, and Extended Fig. 2 for the experimental geometry) [10, 19]. The O *K* XAS spectra also show a good consistency to other infinite-layer nickelates, across the bulk and at the surface of the film, that the hole-peak weight is significantly suppressed at the pre-edge owing to much reduced O 2*p*-Ni 3*d* hybridization (Extended Fig. 3) [10, 11, 20]. To begin the search for symmetry-breaking orders, we performed momentum-dependent RIXS on NNO₂-1 (*σ* polarisation is used throughout unless otherwise stated). By exciting at the Ni *L*₃ resonance (A in Fig. 1b), quasielastic scattering peaks appear at *q*_{||} = ±0.333 *r.l.u.*

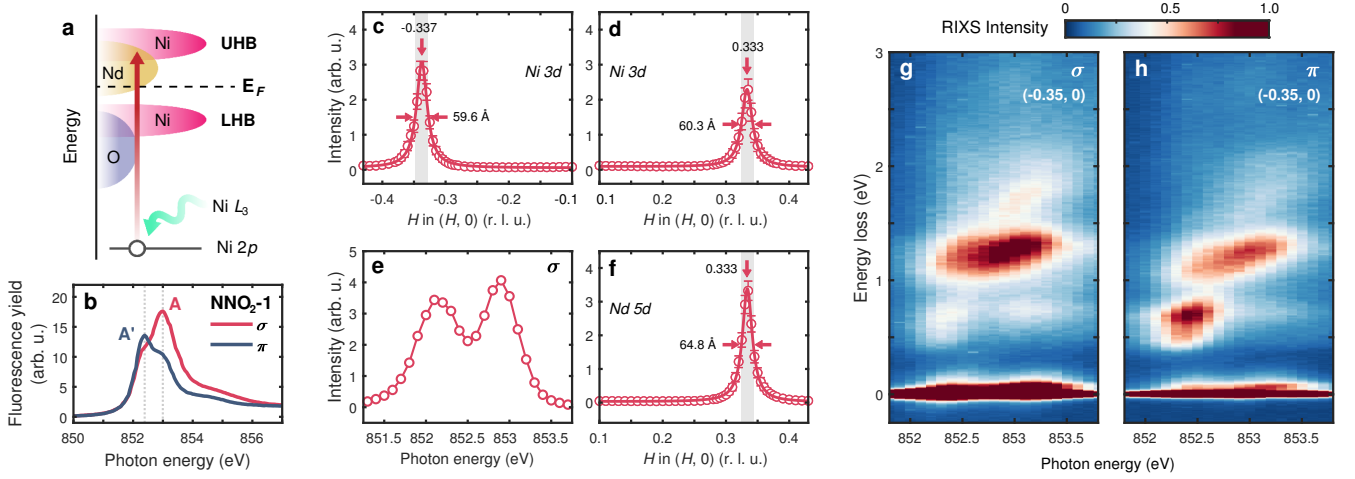


FIG. 1. **CDWs in the parent NdNiO₂ thin film NNO₂-1.** **a**, Schematic electronic structure of the infinite-layer nickelates. **b**, Ni L_3 XAS of the parent NdNiO₂ film NNO₂-1. **c** and **d**, The integrated quasielastic peak intensity as a function of the momentum transfer along $(\pm H, 0)$ direction by exciting at the Ni $3d$ resonance (A peak in **b**). The sign of the momentum transfer is defined in Methods (See also Extended Fig. 2). **e**, The resonant energy profile of the CDW by fixing the momentum transfer to $Q_{CDW} = (+0.333, 0)$. **f**, The integrated quasielastic peak intensity as a function of the momentum transfer along $(H, 0)$ direction by exciting at the Nd $5d$ resonance (A' peak in **b**). **g** and **h**, RIXS maps with photon energy varied across the Ni L_3 -edge on NNO₂-1 at 20 K at $h = -0.35$ r.l.u. with σ and π incident x-ray polarisation, respectively.

along the primary $(H, 0)$, *i.e.*, the Ni-O bonding direction (Fig. 1c and d). Scanning the (H, H) direction however did not reveal such peaks (Extended Fig. 4a). To clarify the origin of the scattering peak, we fixed q_{\parallel} to $+0.333$ r.l.u. and swept the incident photon energy across the Ni L_3 absorption edge. Interestingly, a pronounced double-resonance profile is found coinciding with the two absorption peaks (Fig. 1e). Similar photon energy scan at $q_{\parallel} = -0.35$ r.l.u. across the Ni L_3 shows that the quasielastic peak signal is much stronger in σ than π polarisation indicating the scattering peak has predominantly charge character. In addition, momentum-dependent RIXS scans off Ni L_3 resonance, taken at 840 eV, returned negligible quasielastic scattering peaks (Extended Fig. 4b). The above results suggest that the observed quasielastic scattering peak is attributed to CDW symmetry-breaking order. Notably, the double resonance behaviour contrasts to the CDWs in cuprates where typically a singular resonance profile exists at the Cu L_3 edge [21, 22].

For the infinite-layer nickelates, density-functional theory uncovered there is sizable Ni $3d_{3z^2-r^2}$ mixing with the rare-earth $5d_{3z^2-r^2}$ and $5d_{xy}$ states that leads to 3D Fermi surface pockets that slightly hole dope the half-filled Ni $3d_{x^2-y^2}$ band [8, 12, 23]. As a result, the Ni $3d_{3z^2-r^2}$ weight appears near E_f , although Ni $3d_{3z^2-r^2}$ orbital is furthest away from the Ni $3d_{x^2-y^2}$ orbital in the simplified ligand field picture. The pre-peak in the Ni L_3 XAS spectra as well as the ~ 0.6 eV energy loss feature in RIXS acquired in both σ and π polarisations are the signatures of the hybridized Nd $5d$ -Ni $3d$ orbitals containing

$5d_{3z^2-r^2}$ - and $5d_{xy}$ - symmetries unique for infinite-layer nickelates (Fig. 1b, g and h). We thus positioned the photon energy at the Nd $5d$ resonance (A' in Fig. 1b) and scanned the $(H, 0)$ direction. Remarkably, a quasielastic scattering peak appears at exactly the same wavevector as those at the Ni $3d$ resonance (Fig. 1f). Moreover, the CDW quasielastic peaks at Nd and Ni resonances show comparable half width at half maximum (HWHM) $\Gamma \sim 0.01$ r.l.u., corresponding to a correlation length $(1/\Gamma)$ of ~ 60 Å (Figs. 1d and f). The above results evidence unambiguously that both Nd $5d$ and Ni $3d$ valence charges form density waves in NNO₂-1 propagating with the same period.

To explore the properties of CDWs in infinite-layer NdNiO₂, we designed additional NdNiO₂ thin films by tuning the annealing temperature (See Methods). The new films have c-axis lattice constants comparable to the values commonly obtained (Extended Fig. 1) [1]. Figs. 2a-f summarize the Ni L_3 XAS of the two new NdNiO₂ (denoted as NNO₂-2, and NNO₂-3, hereafter) together with that of NNO₂-1. The two-peak structure is clearly present in all XAS spectra projected along the direction of the in-plane, I_{ab} , and the out-of-plane, I_c (See Methods). Considering NdNiO₂ as a nominal d^9 system, we fitted the two peaks of the projected XAS spectra from which the Nd $5d$ and Ni $3d$ orbital occupancy can be extracted (See Methods). The Nd $5d_{3z^2-r^2}$ and Ni $3d_{3z^2-r^2}$ orbital content is thus defined as $I_c / (I_c + I_{ab})$. Figs. 2m and n show both Nd $5d_{3z^2-r^2}$ and Ni $3d_{3z^2-r^2}$ orbital contents decrease progressively signalling a reduced Nd-Ni hybridization from NNO₂-1 to NNO₂-3.

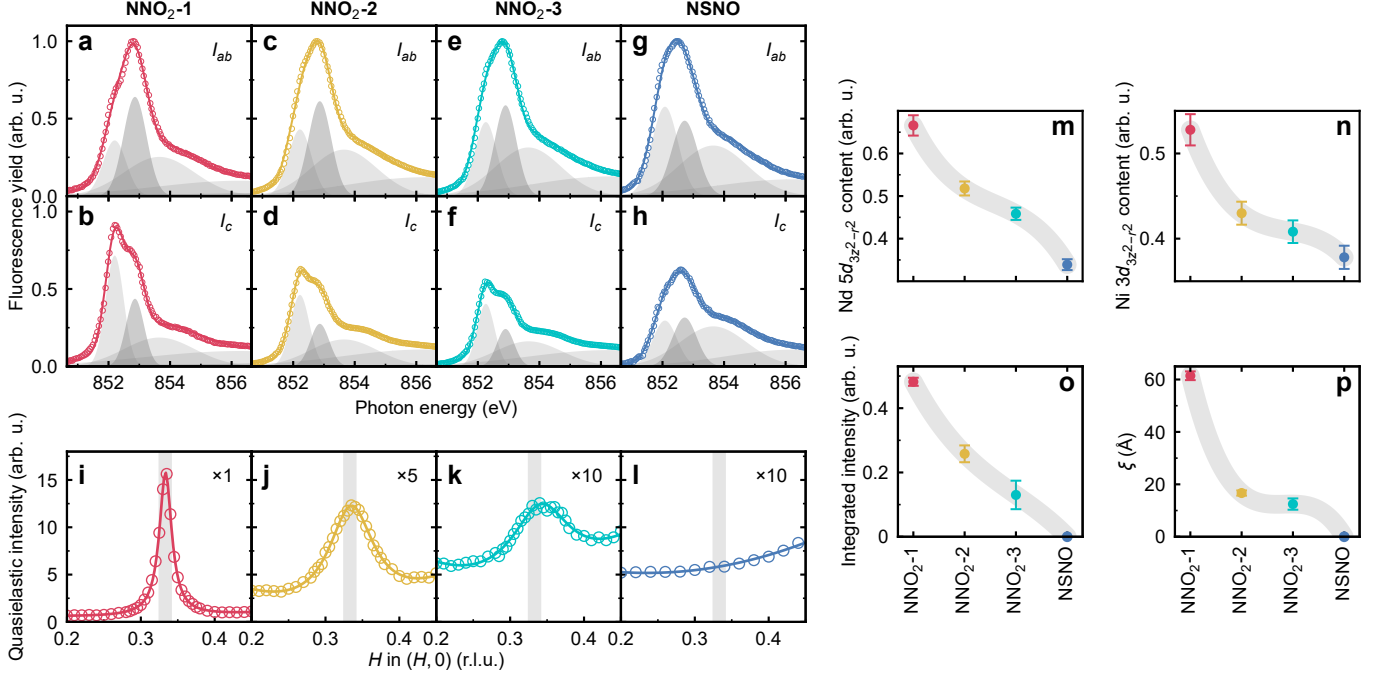


FIG. 2. **Nd 5d-Ni 3d orbital hybridization and CDW in NdNiO₂ and superconducting Nd_{0.8}Sr_{0.2}NiO₂ thin films.** The XAS projected in (out of) the NiO₂ planes, I_{ab} (I_c), of NNO₂-1, NNO₂-2, NNO₂-3, and NSNO are shown in **a** (**b**), **c** (**d**), **e** (**f**), **g** (**h**), respectively. The fit components that are visible in this energy range are plotted in various shades of grey (See fitting details in Methods). The quasielastic peak intensity showing a CDW in the three NdNiO₂ films are plotted in **i**, **j**, **k**, with no evidence of CDW in NSNO (**l**). The Nd $5d_{3z^2-r^2}$ orbital content (**m**), the Ni $3d_{3z^2-r^2}$ orbital content (**n**), the CDW integrated intensity (**o**), and the CDW correlation length (**p**) show similar trends.

The same monotonic trend is found from the surface layers of the samples (See the total electron yield Ni L_3 XAS in Extended Fig. 5). Conversely, the O K -XAS spectra are consistent across the three samples from the bulk and the surface layers (Extended Fig. 3). RIXS maps of NNO₂-2 and NNO₂-3 also manifest qualitatively the same dd excitations as those in NNO₂-1 (Extended Fig. 6). The consistent spectroscopic results between the bulk and the surface suggest that the variation of the Nd-Ni hybridization results from NdNiO₂ thin films and rule out the possibility of the secondary phases usually built up at the top surface layers [24]. Figs. 2i-k summarise the integrated quasielastic peak intensities as a function of q_{\parallel} along the $(H, 0)$ direction showing clearly CDWs in all samples. To make a quantitative assessment, we fitted the CDW peaks and extracted the intensity and the HWHM (Γ). Figs. 2o and p displays monotonically decreasing CDW integrated intensity and the correlation length, respectively, from NNO₂-1 to NNO₂-3. A similar trend between CDWs and the $d_{3z^2-r^2}$ orbital content across three parent NdNiO₂ suggests that CDWs may hold an intimate connection with the Nd-Ni hybridization (Figs. 2m-p). Noticeably, the CDWs in NdNiO₂ are commensurate propagating along the Ni-O bonding direction, distinct to the charge order formed along the Ni-

Ni bonding direction in both single-layer $\text{La}_{2-x}\text{Sr}_x\text{NiO}_4$ and trilayer $\text{La}_4\text{Ni}_3\text{O}_8$ nickelates [25, 26].

We also studied a superconducting Nd_{0.8}Sr_{0.2}NiO₂ film, with a T_c of 10 K (referred as NSNO hereafter). XAS and RIXS measurements were conducted under the same experimental geometry. Whereas NSNO presents similar O K XAS spectra compared to the parent samples (Extended Fig. 3), the Ni L_3 I_c XAS changes noticeably such that the Nd resonance peak becomes much reduced. Comparing to the parent samples, both the Nd $5d_{3z^2-r^2}$ and Ni $3d_{3z^2-r^2}$ orbital content decreases, indicating the Nd-Ni hybridization is further reduced in the superconducting sample (Figs. 2m and n). This is in line with the fact that 20% Sr doping depletes most of the itinerant Nd $5d$ electron carriers [2, 3]. Interestingly, no CDW signals were detected along either $(H, 0)$ or (H, H) directions (Fig. 2l and Extended Fig. 4c). These results of the parent and the superconducting samples suggest that the Nd $5d$ hybridized orbital actively contributes to the CDW ordered states in the infinite-layer nickelates. The situation is disparate to cuprates where the conventional CDWs are solely hosted in the CuO₂ layers, not in the spacer-layers, and are quasi 2D-like [27, 28].

To further explore the properties of CDWs in the infinite-layer nickelates, we examined the L -dependence.

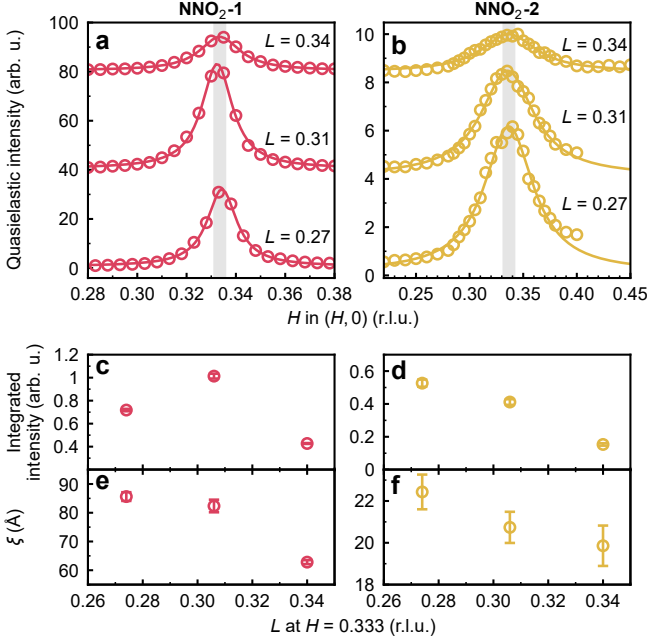


FIG. 3. L -dependence of CDW in NdNiO₂. **a**, and **b**, The integrated quasielastic peaks and their Lorentzian fits along $(H, 0)$ direction with each acquired at a different Ω value for NNO₂-1 and NNO₂-2, respectively. Ω was chosen such that the CDW scattering is peaked at $H = 0.333$ with the corresponded L value labeled in **a** and **b**. Measurements at successively higher L values have been offset for clarity. **c**, and **d**, The integrated intensity of the CDW peak as a function of L at $H = 0.333$. **e**, and **f**, The correlation length of the CDW as a function of L . Error bars in **c-f** are from the least squares fitting.

Fig. 3 displays the series of CDW scans peaked at $(0.333, 0, L)$ from both NNO₂-1 and NNO₂-2 in which L is changed discretely (See Methods). Notably, the CDW peak width and the correlation length change significantly when L is decreased from 0.34 to 0.27. Due to the limit of the Ni L_3 resonance energy and a relatively short c -axis lattice parameter, only a very small portion of the L space is accessible. Nevertheless, the non-negligible L -dependence implies CDWs may have a 3D-like nature. Further studies using hard x-ray scattering may shed light on the dimensionality of the observed CDWs.

We finally performed temperature-dependent RIXS measurements to understand the characteristic temperature of the CDW. Figs. 4a and b displays staggered CDW peaks of NNO₂-1 and NNO₂-2, respectively. The temperature-dependent CDW intensities decay exponentially from which a critical T_{CDW} was obtained (Fig. 4c), however, no noticeable change occurred for the correlation length (Fig. 4d). Upon increasing temperature, the CDW intensity decays to a persistent non-zero intensity up to 300 K, similar to the dynamical CDW fluctuations in cuprates [29–31]. It is remarkable that the stronger

CDWs retain a higher critical temperature T_{CDW} as illustrated in Fig. 4e.

Thus far, we have experimentally confirmed the existence of CDWs in infinite-layer NdNiO₂ films. More importantly, the involvement of Nd $5d_{xy}$, Nd $5d_{3z^2-r^2}$ and Ni $3d_{x^2-y^2}$ orbitals in the formation of CDWs clearly demonstrates that a minimal multi-orbital model is required to describe the low-energy physics of the infinite-layer nickelates [8, 12, 23, 32]. For cuprates, the low-energy physics primarily invokes the hybridized Cu $3d$ and O $2p$ orbitals within the CuO₂ planes although a multi-orbital model is indispensable [22]. Also, unlike conventional CDWs prevalent in the under- or optimally-doped cuprates [28], the CDWs are persistent in parent infinite-layer NdNiO₂ films. This, at first sight, may seem incompatible with the half-filling condition, however, the parent compound is slightly self-doped and metallic-like mimicking a very underdoped state [8, 10, 12].

A broader question is whether in the infinite-layer nickelates the CDWs are intertwined with other symmetry-breaking orders, such as AFM order, SDW, or the superconducting state, manifested in cuprate superconductors [33]. The missing AFM order may seem connected to the competition with the robust CDW states, however, the exact cause is yet to be explored [13, 14]. Interestingly, a previous RIXS study on STO-capped NdNiO₂ films did not reveal any CDW signals, but rather magnons, while in the current work non-capped NdNiO₂ exhibit robust CDWs without sizable magnetic excitations [16]. These perplexing results suggest STO-capping layers influence the material beyond simple surface protection and call for systematic investigations. Concerning the relationship between CDWs and superconductivity, our studies are insufficient to conclude, although no CDWs are seen in superconducting Nd_{0.8}Sr_{0.2}NiO₂. Future studies on Sr-doped Nd_{1-x}Sr_xNiO₂ with different carrier concentrations are strongly desirable. More speculatively, the involvement of Nd $5d_{3z^2-r^2}$ and Ni $3d_{x^2-y^2}$ orbitals close to the Fermi level resembles the situation in some cuprates where the contribution from Cu $3d_{3z^2-r^2}$ orbital works against superconductivity [34, 35]. If Nd $5d$ states are deemed crucial for the low-energy physics, CDWs may appear more competing than cooperative to superconductivity.

Note added - We became aware of similar works on the other infinite-layer nickelates appeared at the time of the submission (arXiv:2112.02484, arXiv:2112.03341).

APPENDIX

Thin film growth

10 (15) nm thick perovskite NdNiO₃ (Nd_{0.8}Sr_{0.2}NiO₃) thin films were grown on TiO₂-terminated SrTiO₃ (001) substrates by pulsed-laser deposition using a 248-nm KrF

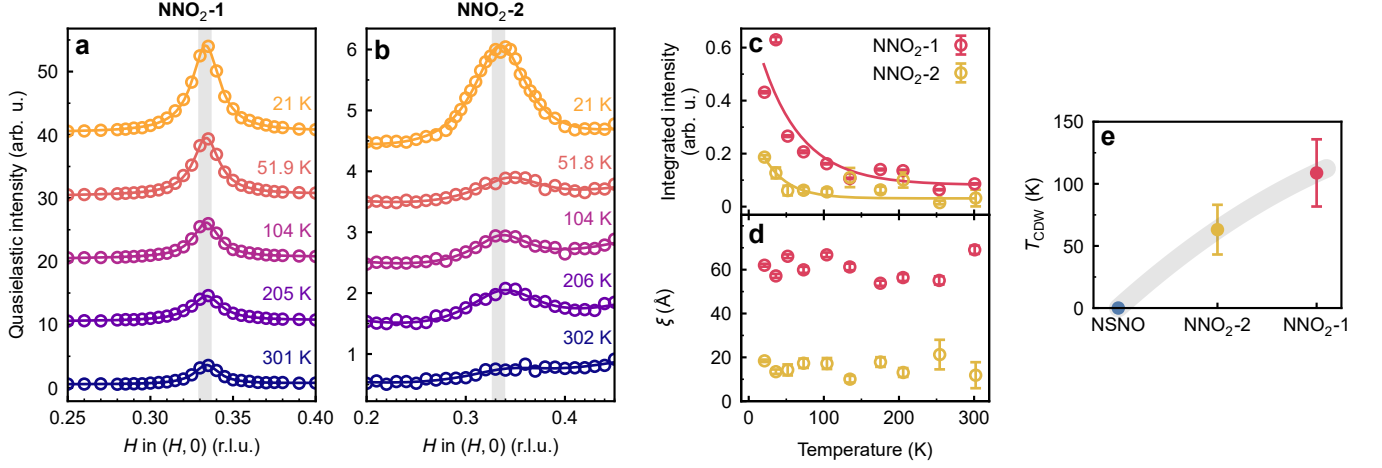


FIG. 4. **Temperature dependence of CDW in NdNiO₂.** **a** (**b**), The CDW peaks and their Lorentzian fits along $(H, 0)$ direction at various temperatures from NNO₂-1 (NNO₂-2). **c**, The integrated CDW intensity as a function of increased temperature. The temperature dependence is fitted with an exponential function (See methods). **d**, The extracted correlation length as a function of increased temperature. **e**, The CDW onset temperature is defined as the temperature where the CDW intensity is at $1/e^2$ for NSNO, NNO₂-2 and NNO₂-1. Error bars in **c-e** are from least squares fitting.

excimer laser. Prior to the deposition, solid state targets were prepared by sintering and pelletizing stoichiometric mixtures of NiO, Nd₂O₃ and SrCO₃ powder at 1300°C for 12 hours. During the deposition, a laser fluence of 1.2 J/cm^2 was used to ablate the target and the substrate temperature was controlled at 620°C with an oxygen pressure of 200 mTorr. All samples do not have SrTiO₃ capping layers. After growth, the thin films were cooled to room temperature under the same oxygen environment. The perovskite samples were reduced to the infinite layer films by following the similar topotactic reduction method in Ref [1]. The perovskite films were vacuum-sealed (pressure ≤ 0.1 mTorr) together with 0.1 gram solid-state redundant CaH₂ powder for a fixed time of 2 hours. Reduction temperatures of 200°C, 220°C, and 290°C were used to produce the NdNiO₂ films denoted NNO₂-1, NNO₂-3, and NNO₂-2, respectively. Nd_{0.8}Sr_{0.2}NiO₃ sample was reduced for a fixed time of 2 hours at a temperature of 300°C. The heating and cooling rate during the reduction process were kept at 10°C/min. NdNiO₂ films crystallize tetragonally and are assumed to have in-plane lattice parameters equivalent to SrTiO₃ $a = b = 3.91 \text{ Å}$. The resistivity was measured by four-probe method via wire-bonded contacts in a cryogen-free magnet system (CFMS, Cryogenic Ltd) down to 1.6 K (Extended Figs. 1a-d). XRD measurements were performed using a monochromatic source Cu K α_1 (Extended Figs. 1e-h).

XAS and RIXS measurements

XAS and RIXS measurements were performed at Beamline I21 at Diamond Light Source, United Kingdom. The crystallographic a - c (b - c) plane of all samples coincided with the horizontal scattering plane shown in Extended Fig. 2. Reciprocal lattice units (r.l.u.) are defined (where $2\pi/a = 2\pi/b = 2\pi/c = 1$) with $\mathbf{Q} = H\mathbf{a}^* + K\mathbf{b}^* + L\mathbf{c}^*$. For all the data presented throughout except for scans in (H, H) , samples were aligned such that $K = 0$. The polar angular offsets (θ and χ) of the films were aligned by specular reflection, and the azimuthal offset (ϕ) by CDW peak, such that the c^* axis was in the scattering plane. The detector arm was at a fixed position of $\Omega = 154^\circ$, unless otherwise stated.

XAS spectra were collected with a grazing incidence angle of $\theta_0 = 20^\circ$ to probe both in-plane and out-of-plane unoccupied states. All measurements were done at a temperature of 20 K with the exit slit opening to $50 \mu\text{m}$ at the Ni L_3 edge except for the temperature-dependent studies. Fluorescence yield XAS spectra were collected with a photodiode and normalised to the incoming beam intensity. Both linearly vertically (σ) and horizontally (π) polarisation were used (Extended Fig. 2). While σ polarised light purely probes the in-plane XAS, *i.e.*, $I_{ab} = I_\sigma$, the out-of-plane XAS were obtained by a combination of both σ and π polarisations with $I_c = (I_\pi - I_\sigma \sin^2[\theta_0]) / \cos^2[\theta_0]$.

Energy-dependent RIXS measurements were performed at an in-plane position of $Q = (-0.35, 0)$ at a temperature of 20 K with the exit slit opening to $30 \mu\text{m}$ corresponding to an energy resolution of 41 meV (FWHM).

The incident energy range went from 851.5 to 854 eV in steps of 100 meV to fully capture the resonance behaviour across the Ni- L_3 absorption peaks.

Momentum-dependent RIXS measurements were performed at resonant energies determined by the absorption peaks in XAS at a temperature of 20 K with the exit slit opening to 40 μm corresponding to an energy resolution of 53 meV (FWHM). To maximise the CDW signal, we used σ polarisation and a grazing out geometry ($\theta > \Omega/2$). L dependent RIXS measurements were done by positioning the spectrometer arm to different Ω angles such that the CDW was always centered at $H = 0.333$ r.l.u.

Data fitting

RIXS data were normalised to the incident photon flux, and subsequently corrected for self-absorption effects, prior to fitting. Energy calibration was obtained by fitting the quasielastic peak to a pseudovoigt with width fixed to instrument resolution and setting the centre of the peak to $E = 0$. The quasielastic peak intensities presented throughout the text were taken by integrating the RIXS spectra in the range $[-27, 27]$ meV.

H dependence of the quasielastic peak intensity was fitted to a Lorentzian. The correlation length was obtained by $\xi = 1/\Gamma$, where $\Gamma = \text{HWHM}$ is the scale parameter of the fitted Lorentzian. To convert from \AA^{-1} to r.l.u., we used the SrTiO_3 lattice parameter $a = 3.91$ \AA . Temperature dependence of the integrated CDW intensity was fitted to an exponential function of the form $I(T; a, b, c) = a \exp(-bT) + c$. The $1/e^2$ intensity was simply $2/b$.

XAS data were normalised to the incident photon flux and then the pre- L_3 -edge intensity was aligned to zero with a fixed intensity at the post-edge for all samples. XAS were collected up to the L_2 -edge and the I_c projection was normalised to the I_{ab} by scaling the L_3 post-edge intensity by a constant factor minimising the difference in intensities by least squares.

The features of the L_3 edge peak and post edge were fitted with four Gaussian peaks and an arctan step function. The centres of the peaks were fixed at approximately 852.2, 853.8, 853.7, and 856.3 eV and the step was fixed at 860.7 eV. Small changes were allowed in the peak centre between samples to improve the reduced χ^2 but were fixed between polarisations of the same sample. From left to right of each XAS spectrum, the width of the first two Gaussians were fixed to each other, and the width of the final Gaussian and step were fixed to each other. All other parameters were left floating. The peaks of interest were centred around ~ 852.2 eV and 852.8 eV. We assigned the lower energy peak to one from Nd-Ni hybridisation and higher energy peak to the $\text{Ni}^{1+} 2p \rightarrow 3d$ transition. The Nd $5d$ and Ni $3d$ orbital contents were

calculated by taking the ratio fitted peak intensities of the out-of-plane XAS and the total fitted peak intensity of both projections, i.e. orbital content $= I_c / (I_c + I_{ab})$. This was done for the Nd-Ni hybridised peak and Ni- L_3 peak separately to determine the Nd $5d_{3z^2-r^2}$ and Ni $3d_{3z^2-r^2}$ orbital content respectively.

* These authors contributed equally

† liang.qiao@uestc.edu.cn

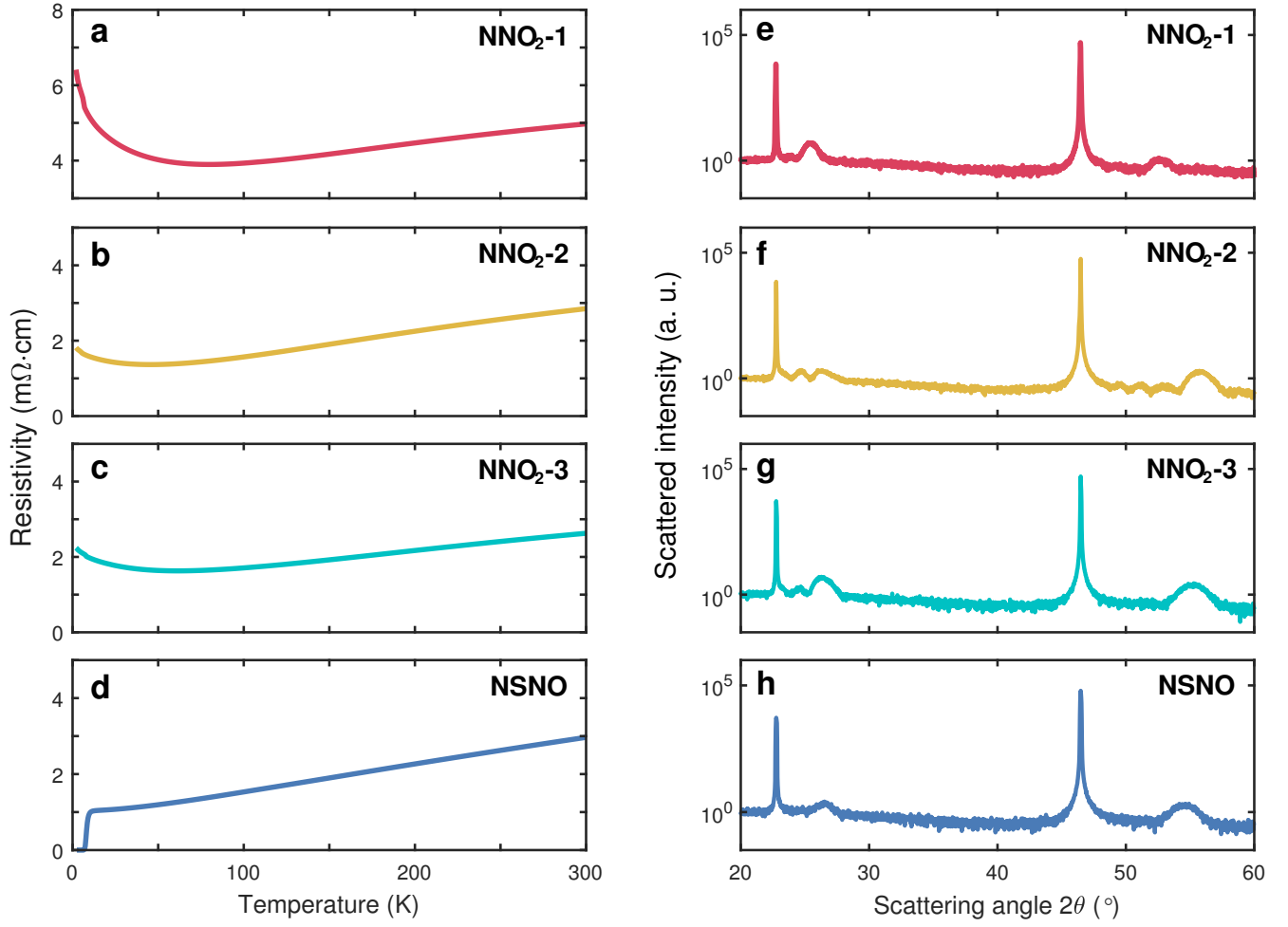
‡ kejin.zhou@diamond.ac.uk

- [1] D. Li, K. Lee, B. Y. Wang, M. Osada, S. Crossley, H. R. Lee, Y. Cui, Y. Hikita, and H. Y. Hwang, Superconductivity in an infinite-layer nickelate, *Nature* **572**, 624 (2019).
- [2] D. Li, B. Y. Wang, K. Lee, S. P. Harvey, M. Osada, B. H. Goodge, L. F. Kourkoutis, and H. Y. Hwang, Superconducting dome in $\text{Nd}_{1-x}\text{Sr}_x\text{NiO}_2$ infinite layer films, *Physical Review Letters* **125**, 027001 (2020).
- [3] S. Zeng, C. S. Tang, X. Yin, C. Li, M. Li, Z. Huang, J. Hu, W. Liu, G. J. Omar, H. Jani, *et al.*, Phase diagram and superconducting dome of infinite-layer $\text{Nd}_{1-x}\text{Sr}_x\text{NiO}_2$ thin films, *Physical Review Letters* **125**, 147003 (2020).
- [4] M. Osada, B. Y. Wang, K. Lee, D. Li, and H. Y. Hwang, Phase diagram of infinite layer praseodymium nickelate $\text{Pr}_{1-x}\text{Sr}_x\text{NiO}_2$ thin films, *Physical Review Materials* **4**, 121801 (2020).
- [5] M. Osada, B. Y. Wang, B. H. Goodge, S. P. Harvey, K. Lee, D. Li, L. F. Kourkoutis, and H. Y. Hwang, Nickelate superconductivity without rare-earth magnetism: $(\text{La}, \text{Sr})\text{NiO}_2$, *Advanced Materials* **33**, 2104083 (2021).
- [6] S. Zeng, C. Li, L. Chow, Y. Cao, Z. Zhang, C. Tang, X. Yin, Z. Lim, J. Hu, P. Yang, *et al.*, Superconductivity in infinite-layer lanthanide nickelates, *arXiv preprint arXiv:2105.13492* (2021).
- [7] V. Anisimov, D. Bukhvalov, and T. Rice, Electronic structure of possible nickelate analogs to the cuprates, *Physical Review B* **59**, 7901 (1999).
- [8] K.-W. Lee and W. Pickett, Infinite-layer LaNiO_2 : Ni^{1+} is not Cu^{2+} , *Physical Review B* **70**, 165109 (2004).
- [9] J. Zaanen, G. Sawatzky, and J. Allen, Band gaps and electronic structure of transition-metal compounds, *Physical Review Letters* **55**, 418 (1985).
- [10] M. Hepting, D. Li, C. Jia, H. Lu, E. Paris, Y. Tseng, X. Feng, M. Osada, E. Been, Y. Hikita, *et al.*, Electronic structure of the parent compound of superconducting infinite-layer nickelates, *Nature Materials* **19**, 381 (2020).
- [11] B. H. Goodge, D. Li, K. Lee, M. Osada, B. Y. Wang, G. A. Sawatzky, H. Y. Hwang, and L. F. Kourkoutis, Doping evolution of the Mott–Hubbard landscape in infinite-layer nickelates, *Proceedings of the National Academy of Sciences* **118** (2021).
- [12] E. Been, W.-S. Lee, H. Y. Hwang, Y. Cui, J. Zaanen, T. Devereaux, B. Moritz, and C. Jia, Electronic structure trends across the rare-earth series in superconducting infinite-layer nickelates, *Physical Review X* **11**, 011050 (2021).
- [13] M. Hayward, M. Green, M. Rosseinsky, and J. Sloan, Sodium hydride as a powerful reducing agent for topotactic oxide deintercalation: Synthesis and characterization

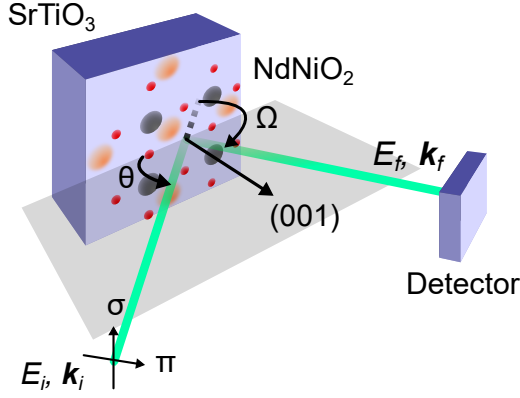
- of the nickel (I) oxide LaNiO_2 , Journal of the American Chemical Society **121**, 8843 (1999).
- [14] M. Hayward and M. Rosseinsky, Synthesis of the infinite layer Ni (I) phase NdNiO_{2+x} by low temperature reduction of NdNiO_3 with sodium hydride, Solid State Sciences **5**, 839 (2003).
- [15] C. Yi *et al.*, NMR evidence of antiferromagnetic spin fluctuations in $\text{Nd}_{0.85}\text{Sr}_{0.15}\text{NiO}_2$, Chinese Physics Letters **38**, 067401 (2021).
- [16] H. Lu, M. Rossi, A. Nag, M. Osada, D. Li, K. Lee, B. Wang, M. Garcia-Fernandez, S. Agrestini, Z. Shen, *et al.*, Magnetic excitations in infinite-layer nickelates, Science **365**, 213 (2021).
- [17] J. Tranquada, B. Sternlieb, J. Axe, Y. Nakamura, and S. Uchida, Evidence for stripe correlations of spins and holes in copper oxide superconductors, Nature **375**, 561 (1995).
- [18] B. Keimer, S. A. Kivelson, M. R. Norman, S. Uchida, and J. Zaanen, From quantum matter to high-temperature superconductivity in copper oxides, Nature **518**, 179 (2015).
- [19] M. Rossi, H. Lu, A. Nag, D. Li, M. Osada, K. Lee, B. Y. Wang, S. Agrestini, M. Garcia-Fernandez, Y.-D. Chuang, *et al.*, Orbital and spin character of doped carriers in infinite-layer nickelates, arXiv preprint arXiv:2011.00595 (2020).
- [20] Z. Chen, M. Osada, D. Li, E. M. Been, S.-D. Chen, M. Hashimoto, D. Lu, S.-K. Mo, K. Lee, B. Y. Wang, *et al.*, Electronic structure of superconducting nickelates probed by resonant photoemission spectroscopy, arXiv preprint arXiv:2106.03963 (2021).
- [21] P. Abbamonte, A. Rusydi, S. Smadici, G. Gu, G. Sawatzky, and D. Feng, Spatially modulated ‘Mottness’ in $\text{La}_{2-x}\text{Ba}_x\text{CuO}_4$, Nature Physics **1**, 155 (2005).
- [22] J. Li, A. Nag, J. Pelliciari, H. Robarts, A. Walters, M. Garcia-Fernandez, H. Eisaki, D. Song, H. Ding, S. Johnston, *et al.*, Multiorbital charge-density wave excitations and concomitant phonon anomalies in $\text{Bi}_2\text{Sr}_2\text{LaCuO}_{6+\delta}$, Proceedings of the National Academy of Sciences **117**, 16219 (2020).
- [23] H. Sakakibara, H. Usui, K. Suzuki, T. Kotani, H. Aoki, and K. Kuroki, Model construction and a possibility of cupratelike pairing in a new d^9 nickelate superconductor (Nd, Sr) NiO_2 , Physical Review Letters **125**, 077003 (2020).
- [24] K. Lee, B. H. Goodge, D. Li, M. Osada, B. Y. Wang, Y. Cui, L. F. Kourkoutis, and H. Y. Hwang, Aspects of the synthesis of thin film superconducting infinite-layer nickelates, Apl Materials **8**, 041107 (2020).
- [25] S.-W. Cheong, H. Y. Hwang, C. Chen, B. Batlogg, L. Rupp Jr, and S. Carter, Charge-ordered states in $(\text{La}, \text{Sr})_2\text{NiO}_4$ for hole concentrations $n_h=1/3$ and $1/2$, Physical Review B **49**, 7088 (1994).
- [26] J. Zhang, Y.-S. Chen, D. Phelan, H. Zheng, M. Norman, and J. Mitchell, Stacked charge stripes in the quasi-2D trilayer nickelate $\text{La}_4\text{Ni}_3\text{O}_8$, Proceedings of the National Academy of Sciences **113**, 8945 (2016).
- [27] G. Ghiringhelli, M. Le Tacon, M. Minola, S. Blanco-Canosa, C. Mazzoli, N. Brookes, G. De Luca, A. Frano, D. Hawthorn, F. He, *et al.*, Long-range incommensurate charge fluctuations in $(\text{Y}, \text{Nd})\text{Ba}_2\text{Cu}_3\text{O}_{6+x}$, Science **337**, 821 (2012).
- [28] R. Comin and A. Damascelli, Resonant x-ray scattering studies of charge order in cuprates, Annual Review of Condensed Matter Physics **7**, 369 (2016).
- [29] H. Miao, J. Lorenzana, G. Seibold, Y. Peng, A. Amorese, F. Yakhov-Harris, K. Kummer, N. Brookes, R. Konik, V. Thampy, *et al.*, High-temperature charge density wave correlations in $\text{La}_{1.875}\text{Ba}_{0.125}\text{CuO}_4$ without spin-charge locking, Proceedings of the National Academy of Sciences **114**, 12430 (2017).
- [30] H. Miao, D. Ishikawa, R. Heid, M. Le Tacon, G. Fabbri, D. Meyers, G. Gu, A. Baron, and M. Dean, Incommensurate phonon anomaly and the nature of charge density waves in cuprates, Physical Review X **8**, 011008 (2018).
- [31] R. Arpaia, S. Caprara, R. Fumagalli, G. De Vecchi, Y. Peng, E. Andersson, D. Betto, G. De Luca, N. Brookes, F. Lombardi, *et al.*, Dynamical charge density fluctuations pervading the phase diagram of a Cu-based high- T_c superconductor, Science **365**, 906 (2019).
- [32] C. Peng, H.-C. Jiang, B. Moritz, T. P. Devereaux, and C. Jia, Superconductivity in a minimal two-band model for infinite-layer nickelates, Preprint arXiv:2110.07593 (2021).
- [33] E. Fradkin, S. A. Kivelson, and J. M. Tranquada, Colloquium: Theory of intertwined orders in high temperature superconductors, Reviews of Modern Physics **87**, 457 (2015).
- [34] H. Sakakibara, H. Usui, K. Kuroki, R. Arita, and H. Aoki, Two-orbital model explains the higher transition temperature of the single-layer Hg-cuprate superconductor compared to that of the La-cuprate superconductor, Physical Review Letters **105**, 057003 (2010).
- [35] Y. Peng, G. Dellea, M. Minola, M. Conni, A. Amorese, D. Di Castro, G. De Luca, K. Kummer, M. Salluzzo, X. Sun, *et al.*, Influence of apical oxygen on the extent of in-plane exchange interaction in cuprate superconductors, Nature Physics **13**, 1201 (2017).

ACKNOWLEDGEMENTS

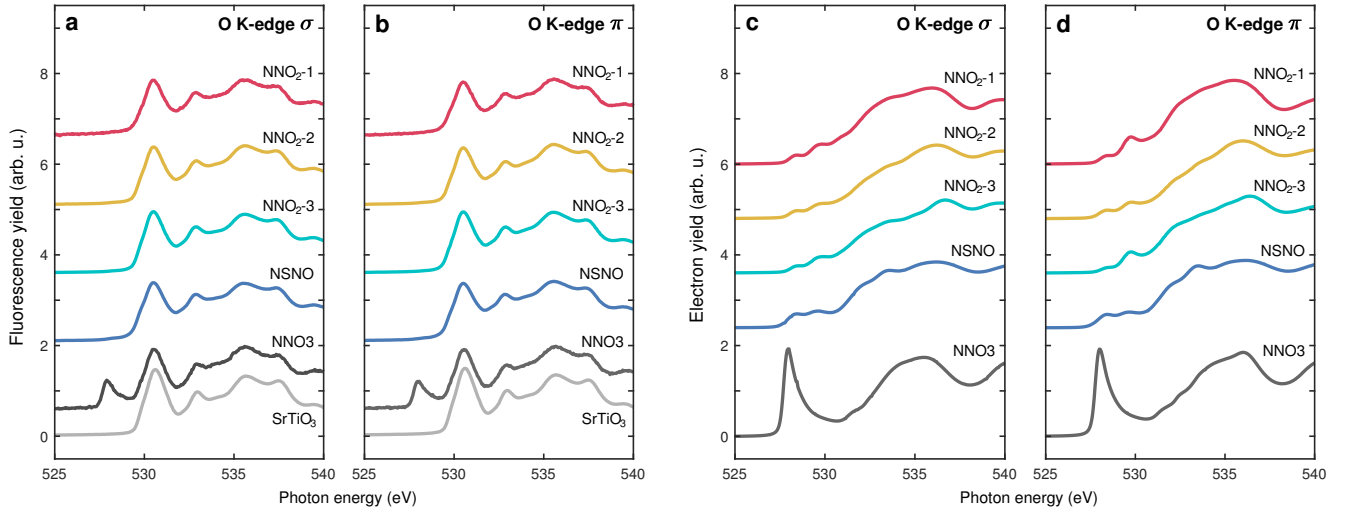
We thank Mark Dean and Wei-Sheng Lee for insightful discussions. All data were taken at the I21 RIXS beamline of Diamond Light Source (United Kingdom) using the RIXS spectrometer designed, built and owned by Diamond Light Source. We thank Diamond Light Source for providing beam time under proposal ID NT30296. We acknowledge T. Rice for the technical support throughout the experiments. L. Q. and H. L. thank the support from the NSFC (Grant Nos. 11774044, 52072059 and 11822411) and SPRP-B of CAS (Grant No. XDB25000000). K.-J.Z. and H.L. thank the support from NSF of Beijing (Grant No. JQ19002).



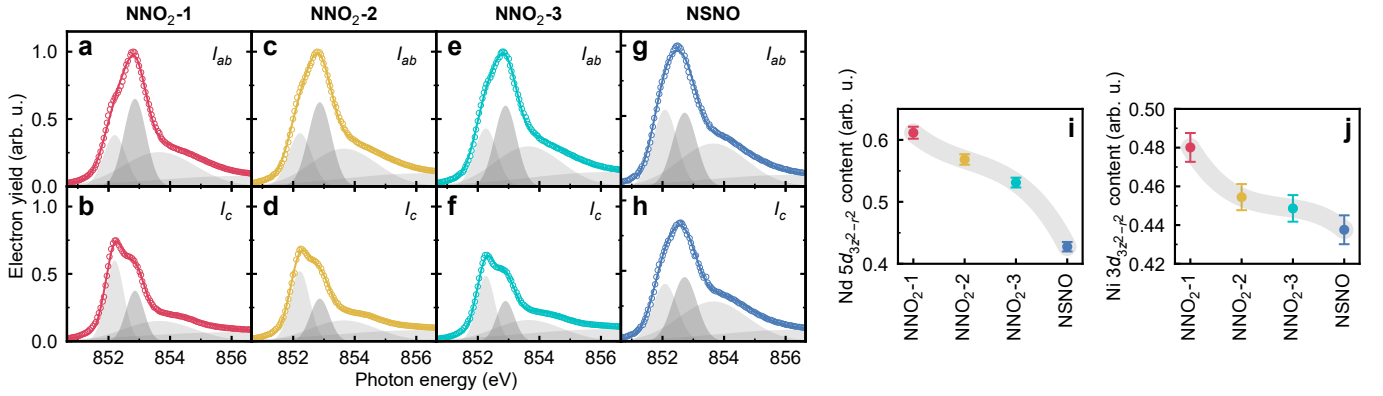
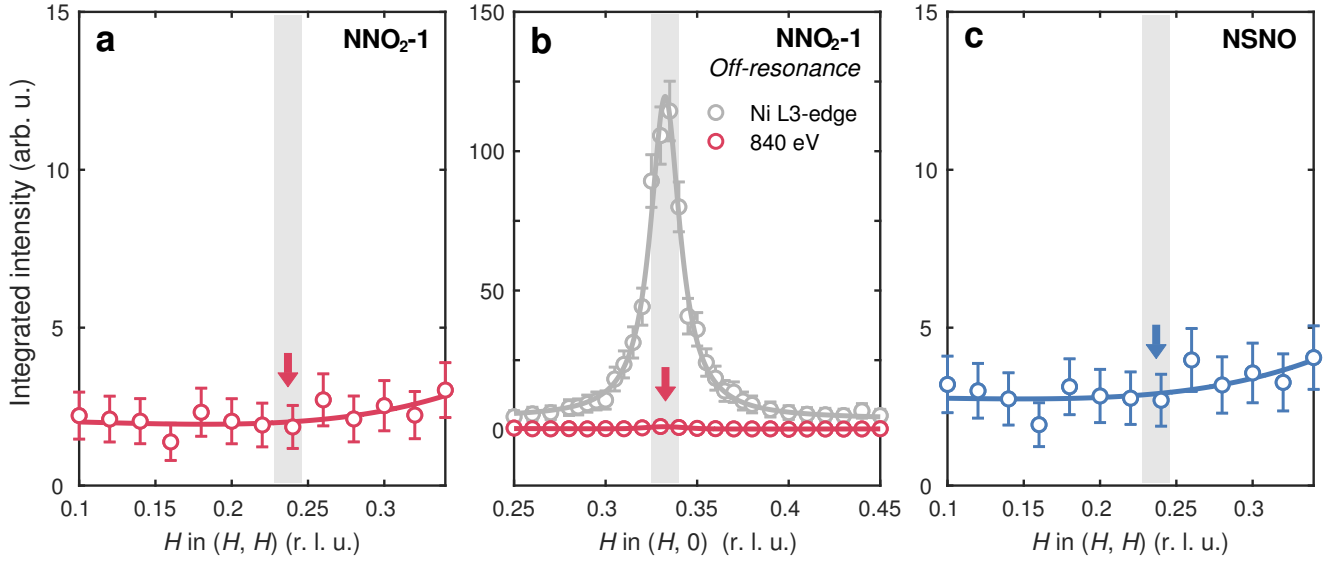
Extended FIG. 1. **Resistivity and XRD data of the parent NdNiO_2 and the superconducting $\text{Nd}_{0.8}\text{Sr}_{0.2}\text{NiO}_2$ thin films.** Note that the parent NdNiO_2 thin films show weakly insulating behaviour and the doped $\text{Nd}_{0.8}\text{Sr}_{0.2}\text{NiO}_2$ has a superconducting onset temperature of about 10 K.

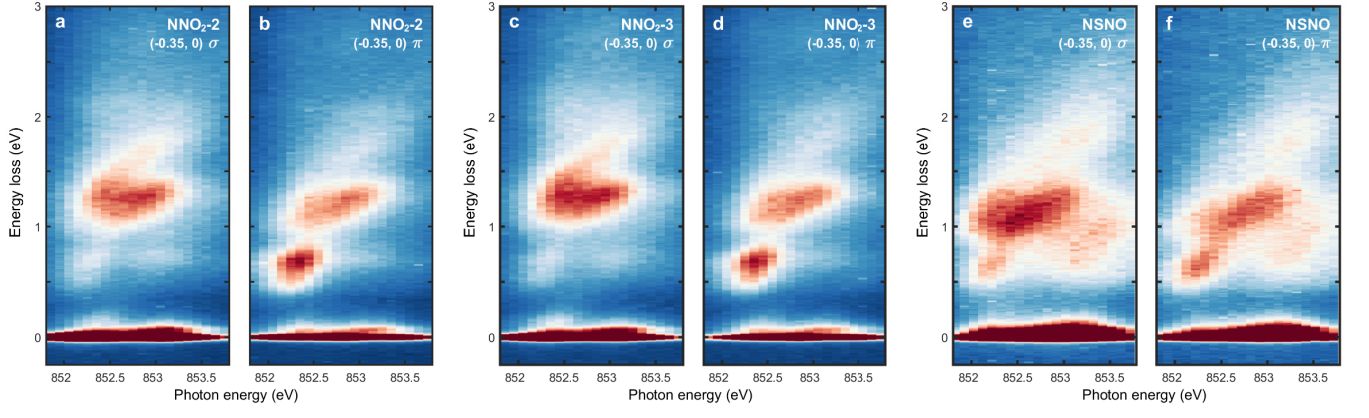


Extended FIG. 2. **The experimental geometry used for the XAS and RIXS measurements.** E_i (E_f) and k_i (k_f) represents the incoming (outgoing) photon energy and momentum, respectively. σ and π stands for the incoming linear vertical and linear horizontal polarisation, respectively. θ is the grazing incident angle between the sample surface and the incoming x-rays while Ω represents the scattering angle of RIXS experiments.



Extended FIG. 3. **O K XAS spectra of thin film samples as well as the as-grown NdNiO₃ thin film.** **a** **(b)**, O K XAS spectra in σ (π) incoming polarisation collected using fluorescence yield representing the signal from the bulk. **c** **(d)**, O K XAS spectra in σ (π) incoming polarisation collected using total electron yield representing the signal from the surface layers. In addition to the main samples, we also present O K XAS data from the reference samples NdNiO₃ (NNO3) for both the electron yield and the fluorescence yield and the O K XAS data from the SrTiO₃ single crystal.





Extended FIG. 6. **RIXS energy maps of $\text{NNO}_2\text{-2}$, $\text{NNO}_2\text{-3}$ and NSNO .** Note that all RIXS maps were collected at $(-0.35, 0)$ in both polarisations.